



# Inactivation of antibiotic resistant bacteria by nitrogen-doped carbon quantum dots through spontaneous generation of intracellular and extracellular reactive oxygen species

Weibo Xia <sup>a,b,1</sup>, Zixia Wu <sup>a,1</sup>, Bingying Hou <sup>a</sup>, Zhang Cheng <sup>b, ID</sup>, Dechuang Bi <sup>a</sup>, Luya Chen <sup>a</sup>, Wei Chen <sup>a,\*\*</sup>, Heyang Yuan <sup>b,\*\*\* ID</sup>, Leo H. Koole <sup>a,\*\*\*\*</sup>, Lei Qi <sup>a,\* ID</sup>

<sup>a</sup> State Key Laboratory of Ophthalmology, Optometry and Visual Science, School of Ophthalmology and Optometry, School of Biomedical Engineering, Eye Hospital, Wenzhou Medical University, Wenzhou, 325027, China

<sup>b</sup> Department of Civil and Environmental Engineering, Temple University, Philadelphia, PA, 19122, United States

## ARTICLE INFO

### Keywords:

Antibiotic resistance  
Carbon quantum dots  
Reactive oxygen species  
Bacterial keratitis  
Antimicrobial activity

## ABSTRACT

The widespread antibiotic resistance has called for alternative antimicrobial agents. Carbon nanomaterials, especially carbon quantum dots (CQDs), may be promising alternatives due to their desirable physicochemical properties and potential antimicrobial activity, but their antimicrobial mechanism remains to be investigated. In this study, nitrogen-doped carbon quantum dots (N-CQDs) were synthesized to inactivate antibiotic-resistant bacteria and treat bacterial keratitis. N-CQDs synthesized via a facile hydrothermal approach displayed a uniform particle size of less than 10 nm, featuring a graphitic carbon structure and functional groups including -OH and -NH<sub>2</sub>. The N-CQDs demonstrated antimicrobial activity against *Staphylococcus aureus* (*S. aureus*) and methicillin-resistant *S. aureus*, which was both dose- and time-dependent, reducing the survival rate to below 1 %. The antimicrobial activity was confirmed by live/dead staining. In *in vivo* studies, the N-CQDs were more efficient in treating drug-resistant bacterial keratitis and reducing corneal damage compared to the common antibiotic levofloxacin. The N-CQDs were shown to generate intracellular and extracellular ROS, which potentially caused oxidative stress, membrane disruption, and cell death. This antimicrobial mechanism was supported by scanning and transmission electron microscopy, significant regulation of genes related to oxidative stress, and increased protein and lactate dehydrogenase leakage. This study has provided insight into the development, application, and mechanism of N-CQDs in antimicrobial applications.

## 1. Introduction

Following the identification of penicillin in the 1920s [1], a variety of antibiotics have been developed and have greatly improved our ability to combat bacterial infections, saving millions of lives every year [2]. However, the abuse of antibiotics over the past several decades has also resulted in antibiotic resistance, a major public health threat and a new type of contamination facing humanity in the 21st century [3]. In the U.S., around \$55–70 billion are spent annually to mitigate antibiotic resistance, and over 23,000 deaths per year are related to antibiotic

resistant bacteria [4]. Many bacteria have evolved resistance to multiple antibiotics, including the last-resort antibiotic vancomycin. The rise of multidrug-resistant organisms, notably methicillin-resistant *Staphylococcus aureus* (MRSA) [5], is causing global fear that we may return to a pre-antibiotic era [6]. The treatment of antibiotic-resistant bacterial keratitis presents significant challenges, as conventional antibiotics frequently prove ineffective, leading to persistent infections and prolonged inflammation [7]. Higher drug doses or invasive interventions are often required, which heightens the risk of systemic and ocular toxicity [8]. The unique anatomical structure of the eye restricts the

\* Corresponding author.

\*\* Corresponding author.

\*\*\* Corresponding author.

\*\*\*\* Corresponding author.

E-mail addresses: [chenweimd@wmu.edu.cn](mailto:chenweimd@wmu.edu.cn) (W. Chen), [heyang.yuan@temple.edu](mailto:heyang.yuan@temple.edu) (H. Yuan), [koole.leo@gmail.com](mailto:koole.leo@gmail.com) (L.H. Koole), [imdoll@163.com](mailto:imdoll@163.com) (L. Qi).

<sup>1</sup> These authors contributed equally to this work.

application of photothermal and physical therapies, while disruption of the corneal barrier further impairs drug delivery [9]. Consequently, there is an urgent need for the development of new antimicrobial agents that robustly inactivate antibiotic-resistant bacteria [10].

Carbon nanomaterials have been extensively researched as a promising alternative to antibiotics due to their outstanding antimicrobial activity [11]. Bacteria can be inactivated by carbon nanomaterials through several mechanisms, including oxidative stress [12], physical and mechanical damage [13], photothermal and photocatalytic effects [14], lipid extraction [15], inhibition of bacterial metabolism [16], encapsulation and isolation [17], and synergistic effects of all these mechanisms [18]. Among these mechanisms, oxidative stress triggered by reactive oxygen species (ROS) including hydrogen peroxide ( $H_2O_2$ ), hydroxyl radical ( $OH^-$ ), and singlet oxygen ( $^1O_2$ ) is considered robust, owing to its high efficiency and lack of selectivity [12b,19]. Carbon nanomaterials can readily generate ROS by providing external energy. For example, electrocatalytic carbon nanomaterials can catalyze the reduction of oxygen to  $H_2O_2$  via two-electron transfer when the electrode is poised at proper potential [20]. Photocatalytic carbon nanomaterials have been shown to produce  $H_2O_2$ -derived ROS when exposed to light of various wavelengths (e.g. ultraviolet (UV), visible, and near-infrared [21]). It should be noted that these external energy inputs for nanomaterials to exhibit antimicrobial activity are often not available in medical and environmental applications [22]. Advancing carbon nanomaterials capable of inactivating bacteria through spontaneous ROS generation is highly desirable.

Carbon quantum dots (CQDs), a class of carbon nanomaterials smaller than 10 nm, have demonstrated the ability to generate ROS and effectively inactivate bacteria. Recent studies have demonstrated that the synthesis of CQDs retaining the active moieties of ciprofloxacin, combined with copper doping, significantly enhances their antimicrobial activity [23]. Furthermore, the self-luminescent CDs effectively inhibit bacterial growth through rapid electron transfer mechanisms [24]. When exposed to  $H_2O_2$ , CQDs facilitate the production of  $OH^-$ , thereby exhibiting antimicrobial activity against Gram-positive bacteria and their biofilms [13d]. Upon exposure to light, CQDs can also catalyze the generation of  $^1O_2$ , a process that effectively inhibits bacterial growth by impairing crucial biomolecules [12a]. In a recent study, CQDs derived from biogenic polyamines showed bactericidal activity by inducing intracellular ROS [12b]. This raised the question of whether CQDs can spontaneously generate extracellular ROS, which could further enhance antimicrobial efficiency [12b]. Intracellular ROS are reactive oxygen species induced by oxidative stress within bacterial cells, while extracellular ROS are directly generated by the material outside the cells. Such a property can be achieved by doping heteroatoms [25], in particularly different forms of nitrogen (e.g. pyridinic N and pyrrolic N) [26]. In nitrogen-doped carbon nanomaterials, nitrogen defects can act as active catalytic sites to facilitate spontaneous ROS generation [26,27]. For example, cobalt-nitrogen co-doped CQDs have been demonstrated to generate ROS and inactivate bacteria [22b]. Metal-nitrogen structures have also been reported to promote the generation of ROS under dark conditions [28]. Although nitrogen-doped carbon quantum dots (N-CQDs) can generate ROS and exhibit antimicrobial effects without external stimuli, their complex fabrication and reduced activity have constrained their application [29]. It is of practical significance to develop facile methods to synthesize N-CQDs capable of spontaneous generation of extracellular ROS and efficient inactivation of bacteria.

This study aims to synthesize N-CQDs that inactivate bacteria through spontaneous intracellular induction and extracellular generation of ROS. To this end, N-CQDs were synthesized from the nitration of pyrene via a one-step hydrothermal method. Compared with pyrolysis methods in previous studies, the hydrothermal method is facile and can enhance the water solubility of N-CQDs, which is beneficial for medical and environmental applications [22b,30]. The antimicrobial properties of the N-CQDs were evaluated by treating MRSA *in vitro* followed by

biocompatibility tests including cytotoxicity assays and hemolysis tests. The medical potential of N-CQDs was further assessed through *vivo* experiments using a rabbit model to study drug-resistant bacterial keratitis. Bacterial keratitis, which can lead to photophobia, pain, and even vision loss [31], is frequently attributed to MRSA, a primary contributor to this common blinding disease [32]. The findings of this study, including efficient inactivation of multi-drug resistant bacteria *in vitro*, successful treatment of drug-resistant bacterial keratitis *in vivo*, and the ability of the synthesized N-CQDs to spontaneously induce intracellular ROS and generate extracellular ROS, can provide insight into the development and application of biocompatible carbon nanomaterials in medical and environmental fields (See Scheme 1).

## 2. Materials and methods

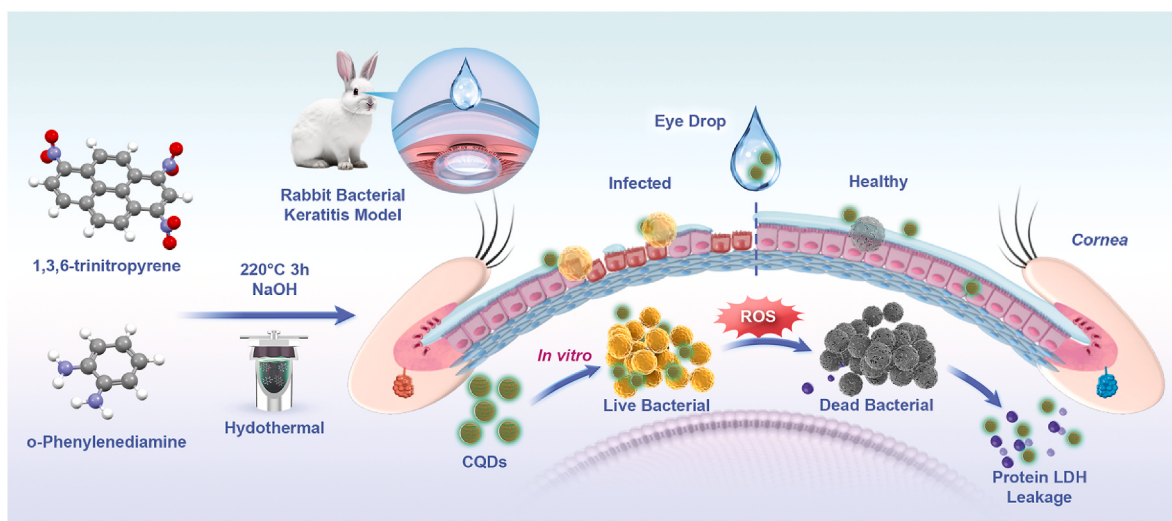
### 2.1. Preparation and characterization of N-CQDs

N-CQDs were synthesized by adapting a technique from the previously literature [33]. In brief, 1,3,6-trinitropyrene (75 mg), o-Phenylenediamine (15 mg) and NaOH (120 mg) in 15 mL of ultrapure water was sonicated for 2 h. This mixture was then placed in a 25-mL Teflon-lined stainless-steel autoclave and heated at 220 °C for 3 h. After hydrothermal processing, the solution was centrifuged at 12,000 rpm for 15 min. The resulting clear brown supernatant was then passed through a 0.22-μm membrane to eliminate remaining particulates. The filtrate solution underwent dialysis in ultrapure water within dialysis bags (molecular weight cut-off 500–1000 Da, Shanghai Yuanye Bio-Technology Co., Ltd) for 24 h to further extract fine particles and residual salts until the pH reached neutral. The final purified N-CQDs powder was acquired through lyophilization.

Stability assessments of N-CQDs at 50  $\mu\text{g mL}^{-1}$  in pure water and DMEM/F12 medium involved extended standing. Morphology and structure were analyzed using high-resolution transmission electron microscopy (HRTEM) (Talos F200X, Thermo Scientific) and atomic force microscopy (AFM, Multimode 8, Bruker Co., Germany). Chemical composition and element states were determined with X-ray photoelectron spectroscopy (XPS) (Escalab 250Xi, Thermo Scientific). Raman microscopy (DXR microscope, Thermo Scientific) at the wavelength of 532 nm at room temperature was utilized to examine the N-CQDs' structure. Fourier transform infrared (FTIR) and UV-visible spectra, recorded by a spectrometer (Nicolet 6700, Thermo Scientific) and a spectrophotometer (Cary 100, Agilent), respectively, assessed chemical structure and functional groups. The crystalline structure was evaluated using X-ray diffraction (XRD) (6000 X-ray diffractometer, Shimadzu). Fluorescence properties were captured with a fluorescence spectrophotometer (F-7000, Hitachi). The free radicals were measured by Electron Paramagnetic Resonance (EPR, Bruker A300, Germany).

### 2.2. In vitro inactivation of bacteria by N-CQDs

Non-resistant *S. aureus* (ATCC 6538) and MRSA (ATCC 43300) were cultured in Luria–Bertani (LB) and Tryptic Soy Broth (TSB), respectively. The pH of the medium was adjusted to pH 6.0 with HCl (1 mol  $L^{-1}$ ) as needed. Colonies were incubated in 5 mL of the respective media at 37 °C and 200 rpm for overnight to achieve logarithmic growth. The antimicrobial activity of synthesized N-CQDs was assessed using the spread plate method. For dose-dependent effects, bacterial cells at  $1 \times 10^6$  CFU/mL were treated with various concentrations of N-CQDs in phosphate-buffered saline (PBS) at 37 °C and 200 rpm for 3 h. Afterward, 50  $\mu\text{L}$  of mixture was plated onto the respective media and incubated at 37 °C for 18 h. Colony counting was performed after incubation. For time-dependent effects, bacterial cells ( $1 \times 10^6$  CFU  $mL^{-1}$ ) were exposed to 5  $\mu\text{g mL}^{-1}$  N-CQDs in PBS at the same conditions for durations of 0–3 h, followed by 18 h on agar plates. Colonies were counted post-incubation. Control groups were cultured in the absence of N-CQDs. A live/dead assay was further performed to evaluate the effects



**Scheme 1.** Schematic Representation of One-Step Hydrothermal Synthesis of N-CQDs from 1,3,6-trinitropyrene and o-Phenylenediamine and Their Antimicrobial Applications.

of synthesized N-CQDs on bacterial cells. The mixture of bacteria cell ( $10^8$  CFU mL $^{-1}$ ) and N-CQDs at 50  $\mu$ g mL $^{-1}$  in PBS at 37 °C, shaking at 200 rpm for 3 h. The mixture was then treated with 4',6-diamidino-2-phenylindole (DAPI) (kit catalog #C1002, Beyotime Biotechnology Co., Ltd) and propidium iodide (PI) staining (kit catalog # C542, DOJINDO Co., Ltd) followed by 30 min of dark incubation. Stained cells were observed with a fluorescence microscope (DMi8, Leica).

### 2.3. In vivo treatment of keratitis with N-CQDs

In vivo experiments utilized male New Zealand White rabbits aged 8–12 weeks (Yuhang Kelian Rabbit Industry Co., Ltd). A rectangular corneal wound with approximately 3 mm in length was established on each rabbit. To establish a bacterial keratitis infection model, 10  $\mu$ L of cell suspension ( $2 \times 10^8$  CFU mL $^{-1}$ ) were applied to the wound. 24 h post-infection, the rabbits were allocated into four groups: (1) control, treated with saline, (2) Levofloxacin-treated, (3) N-CQDs-treated and (4) bacterial keratitis model. Treatment was carried out on Days 0, 1, 3, 5 and 7, and the condition of keratitis was observed using a slit lamp (SLM-8E, Kanghua Co., Ltd) and sodium fluorescein staining. Meanwhile, photographs of the blood agar culture, obtained from corneal secretion extracts, were procured to elucidate the presence of infectious agents. 7 days post-treatment, the rabbits were euthanized, and their corneas were excised, fixed overnight in 4 % paraformaldehyde overnight, dehydrated and embedded in paraffin for histopathological and immunohistochemistry staining. The wax blocks were cut on a paraffin microtome and then dewaxed. Serial sections underwent hematoxylin-eosin staining, and corneal tissue was subjected to immunohistochemistry staining for IL-6 and TNF- $\alpha$ . All procedures were carried out at the Laboratory Animal Center of Wenzhou Medical University, authorized under the license (SYXK (Zhejiang) 2019-0009), complying with China's ethical standards (GB/T 35892–2018) and approval by the Laboratory Animal Ethics Committee (xmsq2022-0236).

### 2.4. Microbial and chemical analyses

Intracellular ROS was quantified with the 2,7-dichlorofluorescein-diacetate assay (catalog #S0033S Beyotime Biotechnology Co., Ltd). Bacteria Cells ( $10^6$  CFU mL $^{-1}$ ) were exposed to 50  $\mu$ g mL $^{-1}$  N-CQDs and incubated at 37 °C, shaking at 200 rpm for 3 h. Both treated and control cells were rinsed with PBS and then incubated in the dark with a 100 mM 2,7-dichlorofluorescein-diacetate in the dark at 37 °C for 30 min. The resultant green fluorescence due to the oxidation of 2,7-

dichlorofluorescein-diacetate to 2,7-dichlorofluorescein, was measured using a microplate reader (SpectraMax190, Molecular Devices) at 485 nm excitation and 528 nm emission.

To characterize bacteria morphology, the bacteria cell-CQDs mixtures were centrifuged at 8,000 rpm for 5 min and resuspended in PBS, maintaining an N-CQDs concentration of 50  $\mu$ g mL $^{-1}$  and a cell concentration of  $10^9$  CFU mL $^{-1}$ . This process was repeated twice. The samples were then fixed with 2.5 % glutaraldehyde at 4 °C for 12 h, followed by stepwise dehydration using ethanol concentrations of 30 %, 50 %, 70 %, 90 %, and 100 %. Finally, cell morphology was analyzed with scanning electron microscopy (SEM) (Phenom ProX, Thermo Scientific) and transmission electron microscopy (TEM) (Talos F200X, Thermo Scientific).

The effect of N-CQDs on cell integrity was assessed by measuring protein and lactate dehydrogenase (LDH) leakage. Cells ( $1 \times 10^6$  CFU mL $^{-1}$ ) were incubated with increasing concentrations of N-CQDs for 3 h at 37 °C. After treatment, the mixture was centrifuged at 8000 rpm for 5 min, and the supernatant was collected and purified by ultrafiltration (molecular weight cut-off = 3000 Da) to remove impurities. Protein concentration in the supernatant was determined using the bicinchoninic acid assay. To measure the leaked LDH, cells were centrifuged again at 8000 rpm for 5 min, the supernatant was discarded and the pellet was washed with PBS. The cells were then incubated with an LDH reaction solution (catalog #CK12, DOJINDO Co., Ltd) in the dark for 30 min. LDH activity was measured using an assay kit (catalog #CK12, DOJINDO Co., Ltd), and the absorbance was read at 490 nm with a microplate reader (SpectraMax190, Molecular Devices).

The biocompatibility of the N-CQDs was evaluated using human corneal epithelial cells (HCECs) cultured in DMEM/F12 at 37 °C with 10 % CO<sub>2</sub>. The culture medium was enriched with 10 % (V/V) certified fetal bovine serum and gentamicin (50 mg mL $^{-1}$ ). Cell viability was assessed using the CCK-8 assay (kit catalog # CK042, DOJINDO Co., Ltd) following the standard protocol. Cells were plated in 96-well plates at a density of  $5 \times 10^3$  cells per well and incubated for 24 h. After incubation, the culture medium was replaced with fresh medium, N-CQDs derivatives at various concentrations were added. The cells were then cultured for an additional 24 h. A live/dead assay was further performed to evaluate the biocompatibility of synthesized N-CQDs on HCECs. HCECs were cultured in 24-well plates at a density of 30,000 cells per well. After 24 h, the cell culture medium was exchanged for fresh medium containing different concentrations of N-CQDs. After 24 h of culture, the cells were stained with Calcein AM (kit catalog #C1430, Invitrogen) and PI staining. Stained cells were observed with a

fluorescence microscope (DMi8, Leica).

For N-CQDs cellular uptake assay, HCECs were cultured on  $10 \times 10$  mm slides in a 24-well plate at 30,000 cells per slide. After 24 h, the medium was replaced with fresh medium containing N-CQDs (100  $\mu\text{g}/\text{mL}$ ). The cells were incubated for 0.5 or 2 h, and nuclei were stained with 7-Aminoactinomycin D (kit catalog #A1310, Invitrogen).

Rabbit blood (2 mL) was centrifuged at 1600 rpm for 5 min to separate the serum and red blood cells (RBCs). The RBCs were washed five times with pre-warmed 10 mM PBS and resuspended in 15 mL of PBS. Subsequently, 400  $\mu\text{L}$  of the RBC suspension was incubated with N-CQDs at concentrations of 5, 10, 20, 50, 100 and 200  $\text{mg mL}^{-1}$  for 2 h at 37 °C, using PBS and deionized water as negative and positive controls. After centrifuging the mixtures at 10,000 rpm for 3 min, the UV-Vis absorbance of the supernatant was measured at 570 nm.

Comparative analysis of gene expression levels between the control and the N-CQDs treated groups was performed based on transcriptomic sequencing. Statistically significant differentially expressed genes were

selected for analysis using a criterion of  $p$ -value  $< 0.05$  and  $|\log_2(\text{fold change})| > 0$ . The differential gene expression analysis was visualized using a volcano plot. An in-depth analysis of differentially expressed genes between the control and treatment groups was performed using the Kyoto Encyclopedia of Genes and Genomes (KEGG) database. The adjusted  $p$ -values ( $\text{padj}$ ) were used to screen the KEGG pathways. Gene ratio was calculated to measure the degree of pathway enrichment by representing the proportion of significant genes within a given pathway relative to the total number of genes in that pathway.

## 2.5. Statistical analysis

All experiments were performed in triplicate, with results expressed as mean  $\pm$  standard deviation. Statistical significance was assessed using an unpaired Student's two-sided  $t$ -test. Significance levels are indicated as follows: \* $p < 0.05$ , \*\* $p < 0.01$ , \*\*\* $p < 0.001$ , and NS indicates no significance.

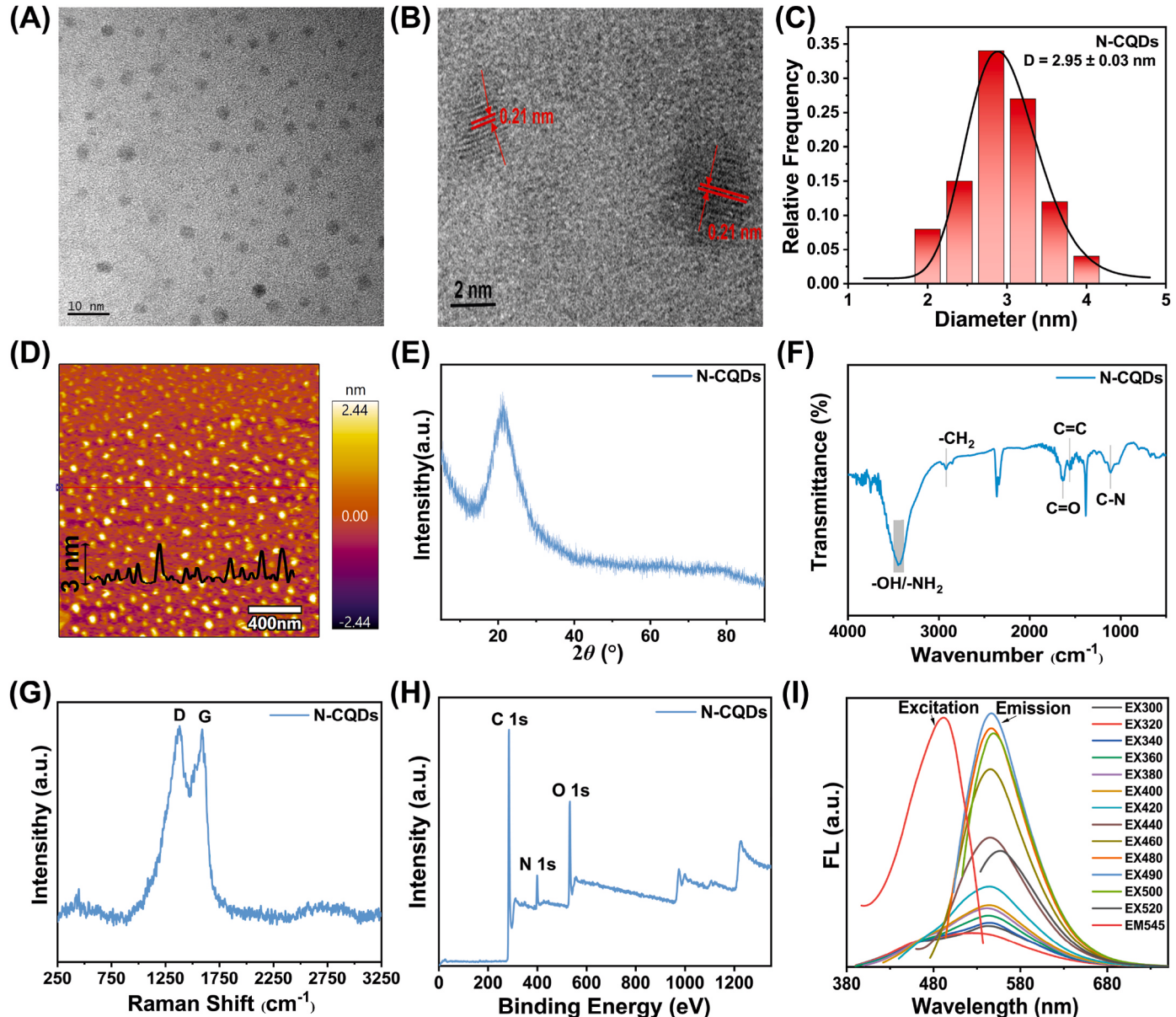


**Fig. 1.** (A) HRTEM image of the N-CQDs. (B) Enlarged HRTEM image of the N-CQDs. (C) Particle size distribution of the N-CQDs. (D) AFM image of the N-CQDs (Inline curve is the selected area for thickness analysis). (E) XRD pattern of the N-CQDs. (F) FTIR spectrum of the N-CQDs. (G) Raman spectrum of the N-CQDs. (H) XPS full survey of the N-CQDs. (I) Fluorescence spectra of the N-CQDs.

### 3. Results and discussion

#### 3.1. Morphology and structure of N-CQDs

Based on previous studies [33], N-CQDs were synthesized with 1,3,6-Trinitropyrene and o-Phenylenediamine as the precursors via a hydrothermal method and subsequently dialyzed in deionized water for 24 h. The enhancement of trinitro reactivity could be related to the three positively charged centers of the NO<sub>2</sub> group, which could potentially facilitate nucleophilic substitution reactions of many basic species, including OH, NH<sub>3</sub>, and NH<sub>2</sub>NH<sub>2</sub>, in hydrothermal media [34]. The introduction of these basic species could enable mass production of water-soluble hydroxyl- and amine-functionalized CQDs.

The synthesized N-CQDs remained as a stable dispersion in deionized water and DMEM/F12 medium for 30 days (Supporting Information (SI) Fig. S1). As shown in Fig. 1A–C, the size distribution of the N-CQDs was relatively uniform, with the particles measured to be less than 10 nm in diameter. The HRTEM image of the N-CQDs showed a lattice spacing of 0.21 nm, which corresponded to the (102) plane of graphitic carbon (Fig. 1B) [35]. HRTEM images of N-CQDs were acquired at pH 6, showing a uniform size, consistent with those observed under neutral conditions (SI Figure S2). The AFM image revealed an average thickness of around 3 nm of the N-CQDs (Fig. 1D). Electrostatic force microscopy (EFM) images reveal the presence of specific carbon defects and electron-rich region within the N-CQDs (SI Figure S3) [36]. The peak at 20.5° observed in the X-ray diffraction (XRD) pattern (Fig. 1E) could be attributed to the (002) plane of graphitic carbon [37]. The graphene structure endows CQDs with superior electronic conductivity, which can enhance the separation efficiency of electron-hole pairs and subsequently promotes the generation of ROS [36a,38].

The N-CQDs were further characterized using spectral analysis. A broad absorption of N-CQDs was observed in UV-visible absorption spectroscopy (SI Figure S4). The absorption peaks at about 240 nm and 330 nm could be attributed to the n-σ\* transition of the conjugated -NH<sub>2</sub> structure and the n-π\* transition of the C=O structure, respectively [39]. The bands observed at 2921, 1737, 1637 and 1383 cm<sup>-1</sup> in the FTIR spectra (Fig. 1F) could be attributed to the stretching/in-plane bending vibration of -CH<sub>2</sub>, -C=O, -C=C and C-N, respectively [40]. The broad bands centered between 3328 and 3354 cm<sup>-1</sup> indicated the presence of -OH and -NH<sub>2</sub>, respectively [41]. The hydroxyl functional groups on the surface of N-CQDs can enhance their water solubility and reactivity, thereby promoting the generation of ROS [38]. The Raman spectra of the N-CQDs (Fig. 1G) exhibited clear peaks at 1375 cm<sup>-1</sup> (the D band) and 1589 cm<sup>-1</sup> (the G band). The I<sub>D</sub>/I<sub>G</sub> intensity value for the N-CQDs was calculated to be 1.22, suggesting the carbon defects and a graphitic structure [42]. Defects in carbon nanomaterials have been reported to induce the generation of ROS by altering the charge distribution [36b, 43]. The XPS spectra confirmed that the N-CQDs contained three main elements (Fig. 1H): C, N, and O. Furthermore, it was found that the N-CQDs contained 76 % C1s (284.8 eV), 16 % O1s (531.23 eV) and 8 % N1s (399.15 eV) (SI Figure S5) [44]. The binding energies of 398.8 eV and 399.9 eV were typically associated with pyrrolic nitrogen and pyridinic nitrogen, respectively [45]. These nitrogen species were commonly found in nitrogen-doped carbon materials, with pyridinic nitrogen being a prevalent nitrogen site [45b]. Previous studies have found that nitrogen-doping can lead to charge redistribution around adjacent carbon atoms, thereby inducing the generation of ROS [46]. As shown in the fluorescence spectrum image, when excited at a wavelength of 490 nm, the N-CQDs dispersion emits the strongest fluorescence centered at 545 nm (Fig. 1I). Collectively, the results demonstrated the successful synthesis of N-CQDs with uniform size distribution, graphitic carbon structure, and surface functional groups that can enhance water solubility and reactivity and potentially favor ROS generation.

#### 3.2. In vitro antimicrobial performance of N-CQDs

The antimicrobial performance of the synthesized N-CQDs was first evaluated by inactivating *S. aureus* and MRSA *in vitro*. The N-CQDs exhibited dose-dependent antimicrobial activity. When the N-CQDs were used to treat MRSA at pH 7 for 3 h (Fig. 2A), the inactivation efficiency increased from 20 % with 2 µg mL<sup>-1</sup> N-CQDs, to 96 % with 5 µg mL<sup>-1</sup>, and to 100 % at the minimum bactericidal concentration (MBC) of 10 µg mL<sup>-1</sup> (Decreased by three orders of magnitude). Similarly, inactivation of non-resistant *S. aureus* was improved from 13 % over 96 %–100 % as the N-CQDs concentration increased from 2 µg mL<sup>-1</sup> over 5 µg mL<sup>-1</sup> to the MBC of 10 µg mL<sup>-1</sup> (Decreased by three orders of magnitude). The increased susceptibility of MRSA to N-CQDs compared to *S. aureus* may be attributed to the extra metabolic burden and energy demands associated with the acquisition and maintenance of drug-resistant genes [47]. This adaptive adjustment imposes a cost on MRSA, potentially slowing its growth and rendering it more vulnerable to external stressors [47a]. In addition to experiments at pH 7, *in vitro* inactivation experiments were also conducted at pH 6 because the typical pH in medical applications (e.g., tumor and inflammatory microenvironment) is slightly acidic [48]. As shown in SI Figure S6 & S7, N-CQDs consistently exhibited a significant level of antimicrobial activity. The survival rates of MRSA and *S. aureus* were reduced to less than 1 % when treated with N-CQDs at a concentration of 10 µg mL<sup>-1</sup> at pH 6. The antimicrobial efficacy of levofloxacin eye drops against MRSA and *S. aureus* was also evaluated. At a concentration of 100 µg mL<sup>-1</sup>, the survival rates of both MRSA and *S. aureus* remained higher than 20 %. Meanwhile, the results demonstrated that the antimicrobial effect of levofloxacin on MRSA was less effective compared to *S. aureus* (SI Figure S8 and S9) Dose-dependent antimicrobial activity of N-CQDs against MRSA is highly desirable because this variant of *S. aureus* exhibits resistance to several commonly used antibiotics, complicating treatment protocols [47b]. The development of bacterial resistance to N-CQDs by MRSA and *S. aureus* was evaluated. After 12 successive passages, the minimum inhibitory concentration (MIC) of N-CQDs remained constant at 5 µg mL<sup>-1</sup> (SI Figure S10). It's in agreement with the findings from the concentration-dependent antimicrobial assay. The resistance assay indicated that neither MRSA nor *S. aureus* exhibited the development of resistance to N-CQDs, which is consistent with the known properties of carbon-based nanomaterials that prevent the emergence of antimicrobial resistance [14b].

The N-CQDs also exhibited time-dependent antimicrobial activity. As can be seen in Fig. 2C and D, the survival rate of MRSA decreased significantly to 80 % and 55 % after 0.5 h and 1 h of treatment, respectively. The survival rate further dropped to 9 % after 2 h of treatment and eventually reached 0 % after 3 h of treatment. Similarly, the survival rate of *S. aureus* reduced slightly to 92 % at 0.5 h, followed by a rapid decrease to 0 % at 3 h (Fig. 2E and F). To further investigate the antimicrobial activity, live/dead experiments were performed by labeling N-CQDs-treated cells using DAPI and PI staining. Live cells can be labeled with DAPI and show blue fluorescence [49], whereas dead cells can be stained by PI with red fluorescence as the dye penetrates damaged cell membranes [50]. Both MRSA and *S. aureus* in the PBS-treated control groups showed prominent blue fluorescence with minimal red fluorescence (Fig. 2G). In contrast, red fluorescence was observed in the N-CQDs-treated groups, confirming the antimicrobial effect of the N-CQDs and implying membrane damage (Fig. 2H). The results collectively demonstrate the potential of N-CQDs in antimicrobial applications, especially in the inactivation of antibiotic resistant bacteria.

#### 3.3. Biocompatibility of N-CQDs

Before the synthesized N-CQDs can be used in medical and environmental applications, it is critical to ensure that they are biocompatible and non-toxic to humans. The biocompatibility of the N-CQDs was

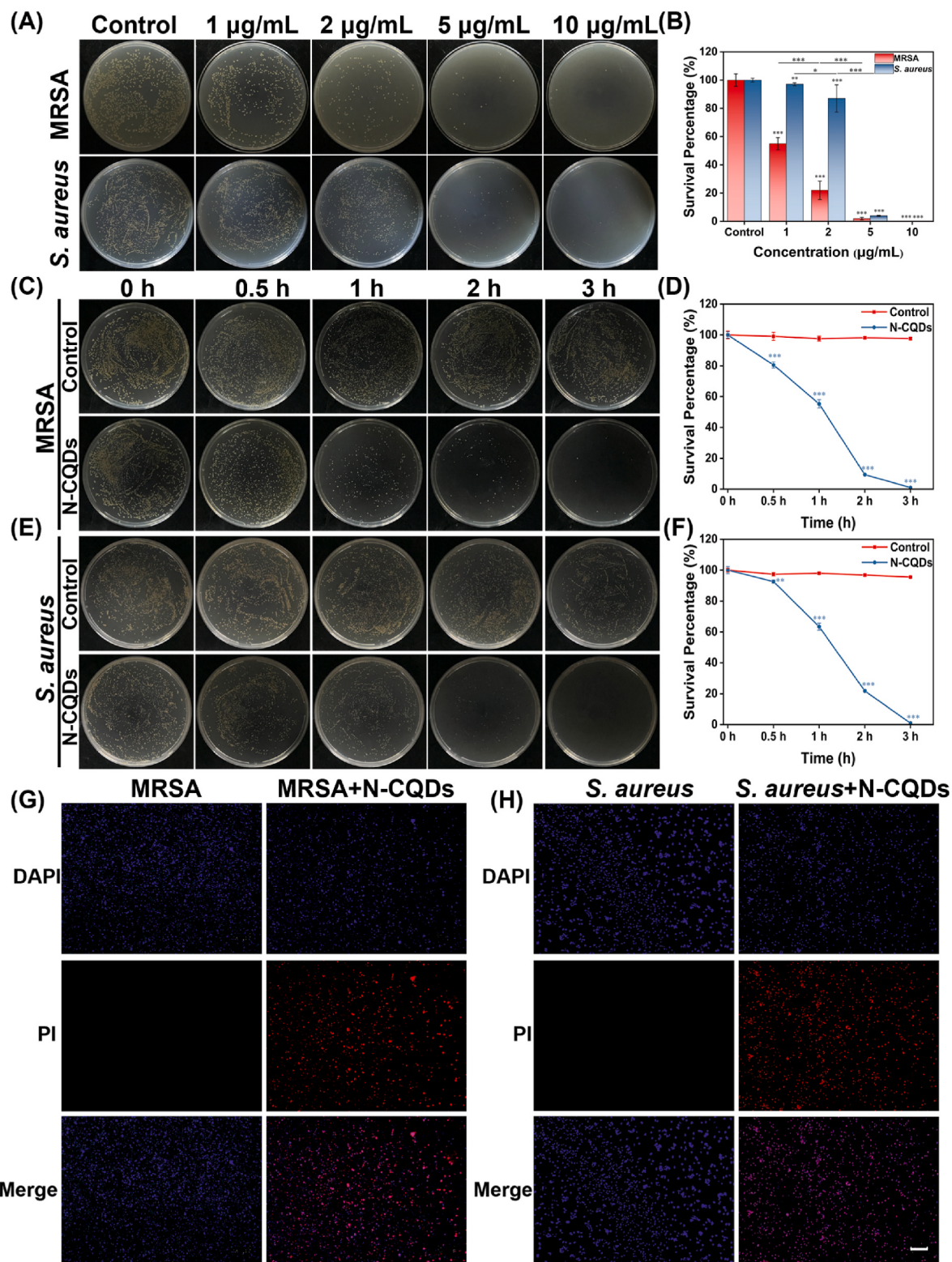


**Fig. 2.** (A) Colonies of MRSA and *S. aureus* treated with different concentrations of N-CQDs (B) Survival percentage of MRSA and *S. aureus* determined by the plate count method. (C) Colonies and (D) survival percentage of MRSA with  $5 \mu\text{g mL}^{-1}$  N-CQDs for different time. (E) Colonies and (F) survival percentage of *S. aureus* treated with  $5 \mu\text{g mL}^{-1}$  N-CQDs for different time. Live/dead fluorescence staining images of control and N-CQDs-treated (G) MRSA and (H) *S. aureus*. Scale bar:  $100 \mu\text{m}$ .

initially assessed through a CCK-8 cytotoxicity assay on HCECs. After 24 h of incubation with N-CQDs concentrations up to  $100 \mu\text{g mL}^{-1}$  (10 times the minimum inhibitory concentration for the tested bacteria), the viability of the N-CQDs-treated HCECs was comparable to that of the

controls and remained at 100 % (SI Figure S11). The biocompatibility of the N-CQDs was also evaluated using a live/dead cell double staining method with calcein-AM/PI. The majority of the cells showed green fluorescence (SI Figure S12), further confirming the low cytotoxicity of

the N-CQDs. The interaction between the N-CQDs and HCECs was examined with confocal microscopy. SI Figure S13 shows that the N-CQDs are located in the cytoplasm of HCECs with a minimal presence observed in the nucleus. The assimilation of the N-CQDs by HCECs might explain the low cytotoxic effects. Finally, the biocompatibility of the N-CQDs was evaluated using *in vitro* hemolysis assays, in which defibrinated rabbit blood was exposed to up to  $100 \mu\text{g mL}^{-1}$  N-CQDs. Regardless of the concentration applied, N-CQDs did not cause hemolysis, and the blood cells remained intact (SI Figure S14). In the *in vivo* safety assessment experiment, pathological H&E staining was performed on tissue sections from the heart, liver, skin, lungs, kidneys, and cornea (SI Figure S15). The histopathological results revealed no significant toxicity or abnormalities. Concurrently, hematological and biochemical analyses were conducted on New Zealand White rabbits (SI Table S1). Blood parameters, as well as liver and renal function markers, in both the control and N-CQDs groups, were within the normal physiological range. Additionally, the corneas of rabbits in the NC and N-CQDs groups were examined using slit-lamp microscopy and evaluated with sodium fluorescein staining (SI Figure S16). Post-administration, the corneas in the N-CQDs group remained clear and translucent, comparable to those in the NC group, with no sodium fluorescein staining observed, indicating that the treatment did not induce corneal damage. In conclusion, a comprehensive series of *in vitro* and *in vivo* biosafety assessments demonstrated that the synthesized N-CQDs exhibit excellent biocompatibility.

### 3.4. *In vivo* antimicrobial performance of N-CQDs

The *in vivo* antimicrobial performance of the synthesized N-CQDs was evaluated with a rabbit model of drug-resistant bacterial keratitis. In the control group, rabbit corneas appeared transparent and lustrous with a deep anterior chamber, and the aqueous humor was clear without discernible aqueous cells (Fig. 3A). As a result, the highest corneal scores were observed in the control group. In contrast, the cornea of the bacterial keratitis group appeared to be gray-white and turbid with the iris and pupil being obscured, and the corneal score was as low as 0 (SI Figure S17 & Table S2). As keratitis progressed during the one-week examination, more severe bacterial infection was observed. Obvious ulcers and even peeling developed in the cornea of the bacterial keratitis group. This occurred because the corneal epithelium and stromal cells were damaged by bacterial toxins, leading to an increase in collagenolytic activity and disruption of the collagen matrix in the infected tissue [51].

The synthesized N-CQDs achieved effective treatment of drug-resistant bacterial keratitis with more rapid antimicrobial activity and minimal tissue damage compared to traditional levofloxacin treatment. Levofloxacin, a broad-spectrum antimicrobial drug commonly used to treat bacterial infections [52], was applied to the rabbit model for comparison. At 72 h post-surgery, the corneal score of the N-CQD-treated group increased from 0 to 3 (SI Figure S17). Only slight tissue damage and edema were observed during keratitis (Fig. 3A). After one week of treatment, the cornea of the N-CQDs-treated group became transparent and shiny with a deep anterior chamber and clear aqueous

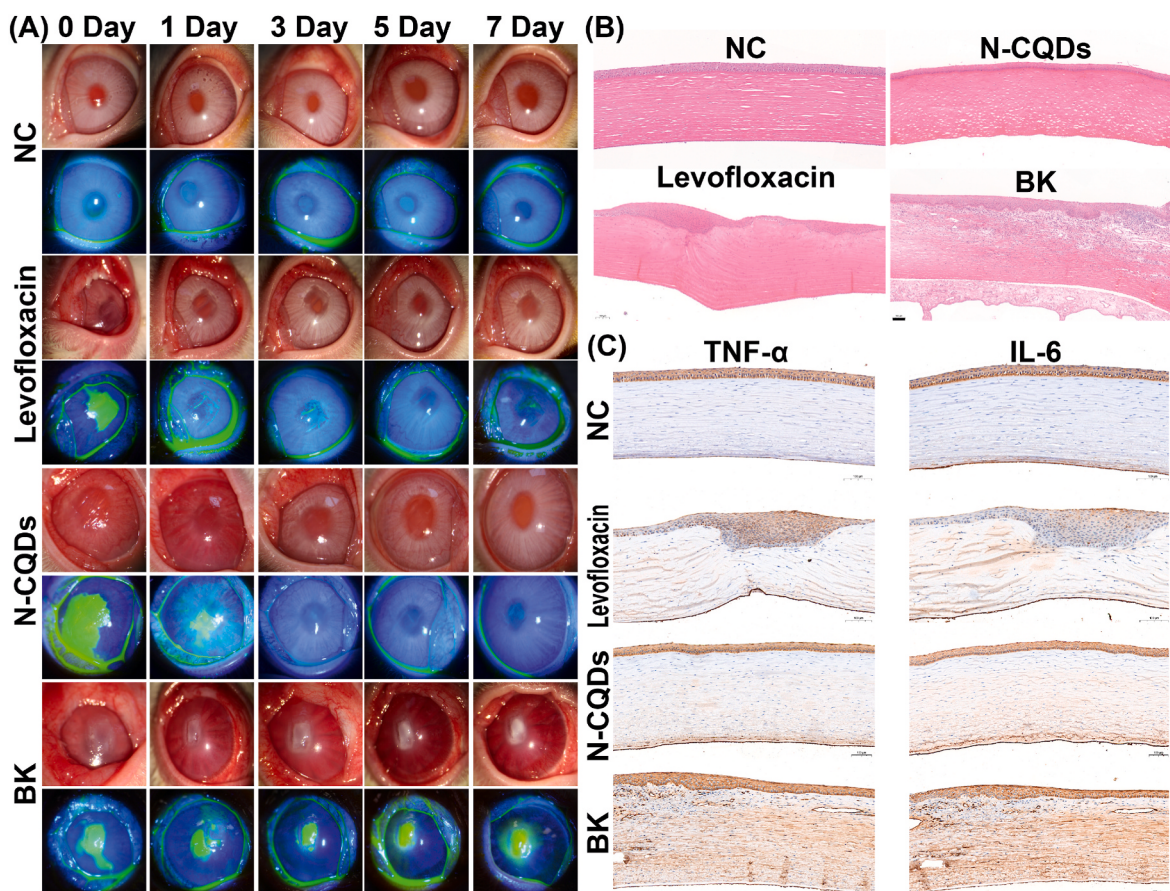


**Fig. 3.** Time-course *in vivo* therapeutic efficacy of after topical instillation of Levofloxacin and N-CQDs eye drops in rabbit drug-resistant bacterial keratitis model. Rabbits that did not undergo surgical treatment and were instilled with PBS served as the blank control group (NC). Rabbits infected with MRSA without any treatment served as the model group of drug-resistant bacterial keratitis (BK). (A) Slit-lamp biomicroscopic images with natural light and cobalt blue light. Follow-up time point: day. (B) Hematoxylin-eosin staining of corneal tissue sections in different groups. Scale bar: 100  $\mu\text{m}$ . (C) Immunohistochemistry TNF- $\alpha$  and IL-6 staining of corneal tissue under different treatment. Scale bar: 100  $\mu\text{m}$ .

humor, and symptoms of inflammation were no longer observed. As a result, the corneal scores of the N-CQDs-treated group recovered to the level of the control group. Within 24 h post-surgery, significant turbidity and obscurity were observed in the cornea and iris, respectively, and a corneal score of below to 2 was recorded in levofloxacin-treated group (Fig. 3A & SI Figure S17). During the subsequent treatment, an improvement in corneal turbidity was observed with slight scars and diminished gloss, but the corneal score remained at 4 since Day 5 (SI Figure S17). In addition to less effective treatment, levofloxacin-based eye drops are often criticized for the need for high doses and frequent application, which may lead to the risk of side effects and the emergence of antibiotic resistance [53].

Sodium fluorescein was used to assess the presence of defects in the cornea. As shown in Fig. 3A, no residual fluorescein sodium was observed in the control, indicating that the cornea was smooth and devoid of defects. In contrast, staining was significant in the bacterial keratitis group. Among the treatment groups, the corneas in the N-CQDs-treated group were found to be clear, transparent, non-stained and intact. However, slight staining was still present in the levofloxacin group. When microbial culture of corneal lesion scrapings was performed on sheep blood agar plates (SI Figure S18), the control and bacterial keratitis groups were found to be negative and strongly positive, respectively, with  $\beta$ -hemolysis rings visible in the bacterial keratitis group. In terms of treatment outcomes, the N-CQDs-treated group consistently showed negative results, whereas the levofloxacin group exhibited trace microbial growth and was weakly positive.

Inflammatory or infectious disorders can cause corneal injury, leading to tissue matrix remodeling and subsequent formation of a disorganized and opaque extracellular matrix [54]. As shown by the hematoxylin-eosin staining results (Fig. 3B), both the control and N-CQDs groups showed a compact corneal structure with uniform thickness and an absence of inflammatory cells. The bacterial keratitis group exhibited a lax corneal structure with pronounced inflammatory

cell infiltration. While the levofloxacin treatment group did not show evident inflammatory cells, the corneal thickness was inconsistent. Drug-resistant bacterial corneal inflammation was further investigated using Immunohistochemistry staining (Fig. 3C). A noticeable decrease in the expression of inflammatory cytokines IL-6 and TNF- $\alpha$  was observed in the N-CQDs group compared to the bacterial keratitis group. These results indicate that the application of the synthesized N-CQDs effectively reduces corneal damage caused by inflammatory injury. In summary, N-CQDs offer a convenient, safe and effective eye drop solution to treat drug-resistant bacterial keratitis.

### 3.5. Antimicrobial mechanism of N-CQDs

For further development and application of N-CQDs in medical and environmental fields, understanding their antimicrobial mechanism is crucial. Many carbon nanomaterials have been reported to inactivate bacteria by inducing intracellular ROS generation [55]. The intracellular levels of ROS in N-CQDs-treated MRSA and *S. aureus* were measured using the 2',7'-dichlorofluorescein diacetate fluorescent dye assay [56]. The fluorescence intensity at 525 nm exhibited a linear correlation with the accumulation of intracellular ROS induced by N-CQDs. As shown in Fig. 4A, the intracellular ROS levels observed in both MRSA and *S. aureus* were comparable to the  $H_2O_2$ -treated positive control and higher than the water-treated negative control. The accumulation of intracellular ROS implies that N-CQDs can cause oxidative stress in MRSA and *S. aureus* when the amount of ROS exceeds the neutralizing capacity of antioxidant systems [57]. Previous studies have demonstrated that ROS are crucial for the antimicrobial effect of the immune system as they inactivate bacteria by damaging their cell membranes, DNA, proteins, and other components [58]. This antimicrobial mechanism has attracted considerable interest due to its potential applications in various fields [59].

In addition to intracellular ROS, extracellular ROS can also

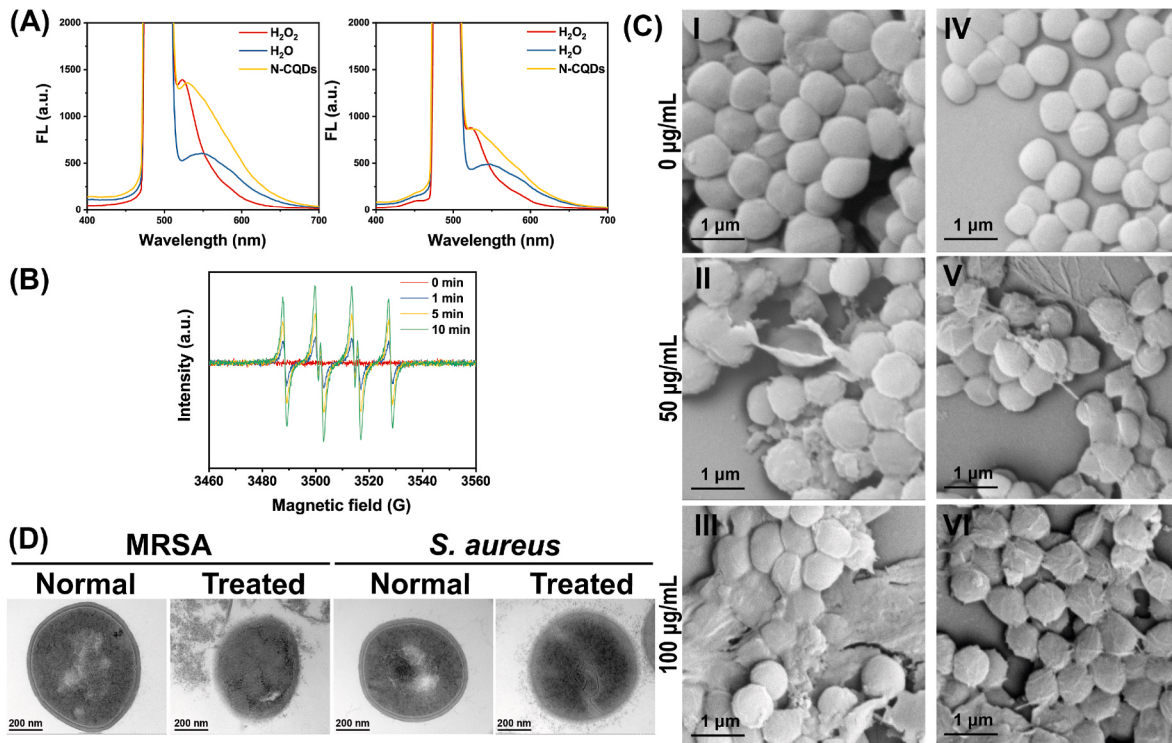


**Fig. 4.** (A) Determination of the ROS generation in MRSA (left) and *S. aureus* (right), bacteria treated with  $H_2O$  and 0.1 mM  $H_2O_2$  as negative controls and positive controls separately. (B) Electron paramagnetic resonance spectra for N-CQDs at different time point under darkness. (C) SEM images of I-III) MRSA and IV-VI) *S. aureus* treated with different concentration of N-CQDs: I) and IV) 0  $\mu\text{g/mL}$ , II) and V) 50  $\mu\text{g/mL}$ , III) and VI) 100  $\mu\text{g/mL}$ . Scale bar: 1  $\mu\text{m}$ . (D) TEM images of normal and treated MRSA and *S. aureus*. Scale bar: 200 nm.

contribute to bacterial inactivation by causing oxidative damage to cell membranes and other vital components. Certain carbon nanomaterials have been reported to generate extracellular ROS, which contribute to their antimicrobial activity [60]. The spontaneous generation of extracellular ROS by the synthesized N-CQDs was further investigated under dark conditions [61]. As shown in Fig. 4B, the electron paramagnetic resonance spectral signal of extracellular ROS increased with longer sampling time, indicating the ability of the N-CQDs to produce extracellular ROS in the absence of external stimuli. Similarly, EPR were further employed to detect hydroxyl radicals (-OH) and singlet oxygen ( $^1\text{O}_2$ ), both of which demonstrated an increase over time, confirming the progressive generation of these reactive oxygen species by the N-CQDs (SI Figure S19). The alterations in absorbance observed in the ABDA and TMB assays further corroborated this finding (SI Figure S20 & S21). Extracellular ROS generation could be attributed to nitrogen doping and intrinsic defects in the carbon material [43], which could function as catalytic sites for extracellular ROS production [46]. Spontaneous generation of extracellular ROS is highly favorable for the antimicrobial applications of N-CQDs.

The nanoscale size of N-CQDs and the induced intracellular ROS can

disrupt bacterial cell membranes and cause leakage of cellular contents [62]. To examine morphological changes in cell membranes caused by N-CQDs, SEM and TEM were performed. In the SEM images (Fig. 4C), the surfaces of untreated MRSA and *S. aureus* exhibited a flat morphology with smooth and intact membrane structures, indicating cell integrity. In contrast, as the concentration of N-CQDs increased, the bacterial skeletal structures of MRSA and *S. aureus* were compromised and the cell membranes ruptured. In the TEM images (Fig. 4D), bacteria treated with N-CQDs exhibit complete disappearance of the membrane structure. To gain an in-depth understanding of ROS-induced cell membrane disruption, protein leakage tests were conducted, and a dose-dependent increase in protein leakage was observed (SI Figure S22). Upon damage to bacterial cell membranes, LDH, a peripheral membrane protein for maintaining intracellular redox equilibrium [63], was released into the culture medium with a dose-dependent increase at higher N-CQDs concentrations (SI Figure S23). Considering the stability of LDH in the environment, the extent of bacterial membrane damage can be reflected by the concentration of released LDH.

To further reveal the effects of the synthesized N-CQDs on cell activity, the gene expression profile of N-CQD-treated MRSA was analyzed.

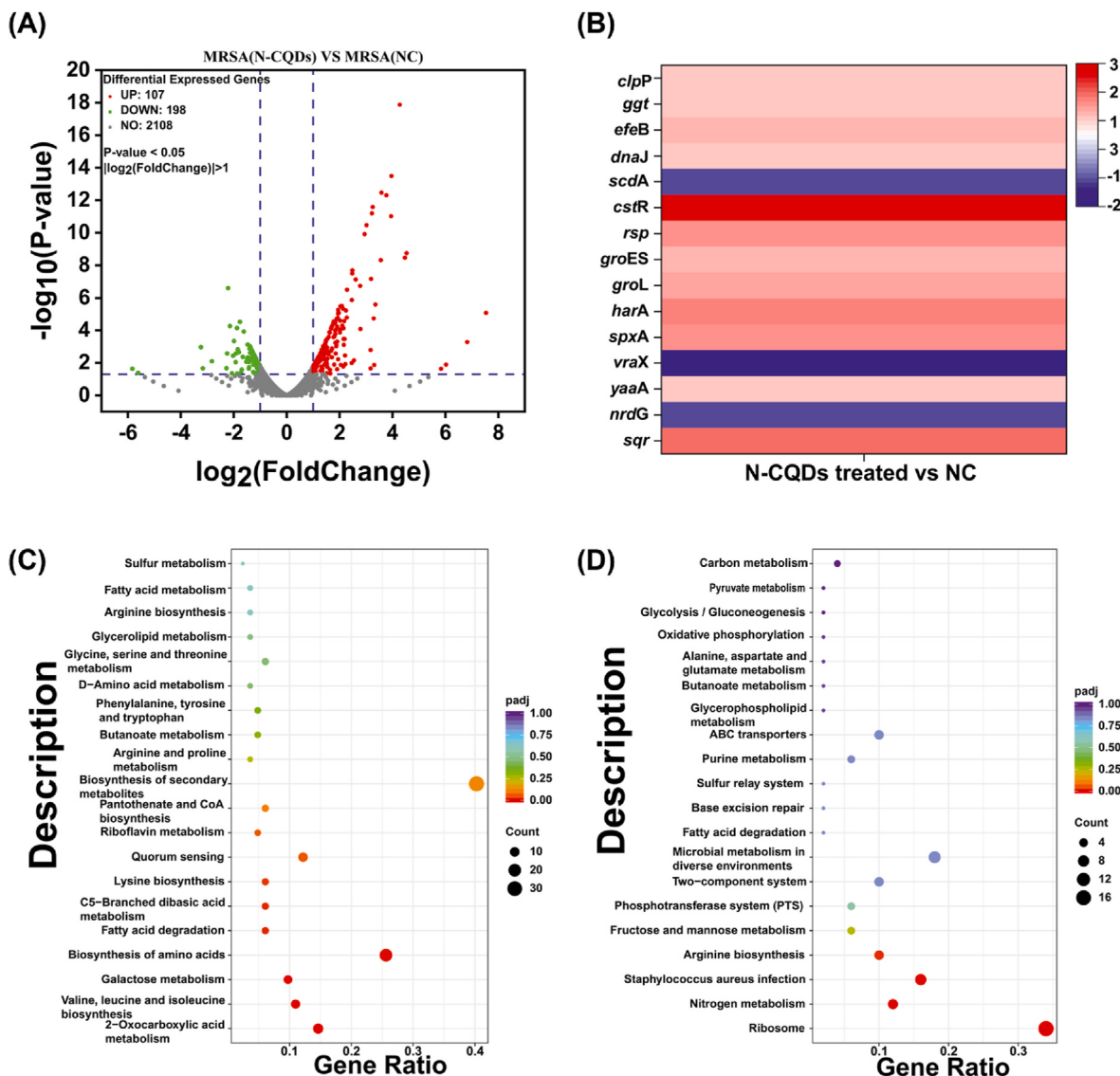


**Fig. 5.** RNA-Seq gene expression profiles of MRSA treated with N-CQDs were compared with the control group. (A) Volcano plot of differentially expressed genes. (B) Heat map analysis of the differentially expressed genes associated with oxidative stress. Top 20 (C) upregulated and (D) downregulated KEGG pathways. padj: adjusted p-value for reducing false positive.

Of the total 305 genes that exhibited differential expression (Fig. 5A), 107 genes were upregulated, and 198 genes were downregulated. Genes related to oxidative stress, including *scdA*, *yaaA*, *spxA*, and *harA* [64], were identified and showed significant regulation (Fig. 5B). Among the top 20 upregulated pathways (Fig. 5C), several could be related to oxidative stress response. For example, sulfur metabolism maybe became more active following treatment with N-CQDs. Given that sulfur can serve as a precursor of glutathione, an essential antioxidant responsible for neutralizing ROS [65], the upregulation of this pathway may be indicative of the cellular response to N-CQDs-induced ROS. Notably, the increased synthesis of secondary metabolites (e.g., antioxidant enzymes) with low padj and high gene ratio indicate was significant, suggesting that it maybe a result of oxidative stress [66]. Similarly, upregulation of fatty acid metabolism with low padj and high gene ratio may also be caused by excessive intracellular ROS, as ROS such as superoxide are produced as by-products during  $\beta$ -oxidation of fatty acids [67]. Meanwhile, critical pathways were found within the top 20 downregulated pathways (Fig. 5D). For example, ribosome pathway had the greatest gene ratio and a very low padj value, and its down-regulation highly probable caused by ROS-induced ribosome impairment [68]. The reduced activity of the phosphotransferase system may adversely affect the pentose phosphate pathway and consequently the production of NADPH [69]. This may impair the maintenance of glutathione in its reduced state for scavenging ROS, making cells more susceptible to oxidative stress [70].

#### 4. Conclusions

In this study, N-CQDs as antimicrobial agents alternative to conventional antibiotics were synthesized using a facile hydrothermal method. The synthesized N-CQDs with uniform size and functional groups enhancing water solubility and ROS generation. *In vitro* antimicrobial tests demonstrated the efficacy of the synthesized N-CQDs in inactivating non-resistant and multidrug-resistant *S. aureus*. Cytotoxicity evaluation revealed high biocompatibility of the N-CQDs. *In vivo* antimicrobial tests demonstrated that the N-CQDs were more efficient than levofloxacin in treating bacterial keratitis caused by multidrug-resistant *S. aureus*. The antimicrobial activity of the N-CQDs was attributed to simultaneous production of intracellular and extracellular ROS. This was supported by cell membrane disruption, leakage of peripheral membrane protein, as well as significant regulation of the genes related to oxidative stress and relevant pathway. Overall, N-CQDs with high biocompatibility and excellent antimicrobial activity may hold great promise in combating antibiotic resistant bacteria.

#### CRediT authorship contribution statement

**Weibo Xia:** Writing – original draft, Data curation, Conceptualization. **Zixia Wu:** Investigation, Formal analysis, Data curation. **Bingying Hou:** Investigation, Data curation. **Zhang Cheng:** Software, Resources. **Dechuang Bi:** Resources, Formal analysis. **Luya Chen:** Validation, Supervision, Resources. **Wei Chen:** Visualization, Validation, Supervision. **Heyang Yuan:** Writing – review & editing, Visualization, Supervision, Conceptualization. **Leo H. Koole:** Visualization, Funding acquisition, Formal analysis. **Lei Qi:** Writing – review & editing, Supervision, Resources.

#### Declaration of competing interest

The authors have no conflicts of interest to declare.

#### Acknowledgment

This work was supported by the U.S. National Science Foundation (Award No. 2307222), the Wenzhou Bureau of Science and Technology (Y20220150), the Medical and Health Technology Project in Zhejiang

Province (2023RC088), the Agricultural and Social Development Science and Technology Plan Project in Yinzhou, Ningbo City (2023AS017), the Ningbo science and technology plan project (2023J211), the project of Ningbo Eye Hospital (2022QN002), the Zhejiang Medical and Health Science and Technology Project (2025KY1458), and the Yinzhou Agricultural and Social Development Scientific Research Project (2023AS017) are acknowledged.

#### Appendix A. Supplementary data

Supplementary data to this article can be found online at <https://doi.org/10.1016/j.mtbiobio.2024.101428>.

#### Data availability

The data that has been used is confidential.

#### References

- [1] E. Martens, A.L. Demain, *J. Antibiot. (Tokyo)* 70 (2017) 520.
- [2] K.H. Luepke, K.J. Suda, H. Boucher, R.L. Russo, M.W. Bonney, T.D. Hunt, J. F. Mohr 3rd, *Pharmacotherapy* 37 (2017) 71.
- [3] a) N.R. Naylor, R. Atun, N. Zhu, K. Kulasanathan, S. Silva, A. Chatterjee, G. M. Knight, J.V. Robotham, *Antimicrob. Resist. Infect. Control* 7 (2018) 58;  
b) M.M. Aljeldah, *Antibiotics* 11 (2022);  
c) European Antimicrobial Resistance, *Lancet Public Health* 7 (2022) e897.
- [4] B. Li, T.J. Webster, *J. Orthop. Res.* 36 (2018) 22.
- [5] a) M. Boolchandani, A.W. D'Souza, G. Dantas, *Nat. Rev. Genet.* 20 (2019) 356;  
b) A.H. Holmes, L.S. Moore, A. Sundsfjord, M. Steinbakk, S. Regmi, A. Karkey, P. J. Guerin, L.J. Piddock, *Lancet* 387 (2016) 176.
- [6] J. Mwangi, X. Hao, R. Lai, Z.Y. Zhang, *Zool. Res.* 40 (2019) 488.
- [7] a) V.S. Chang, D.K. Dhaliwal, L. Raju, R.P. Kowalski, *Cornea* 34 (2015) 698;  
b) Y. Zhang, A. Li, Y. Zhang, S. Hong, Y. Xue, X. Song, J. Li, S. Huang, X. Zhang, *Macromol. Rapid Commun.* 44 (2023) e2300379;  
c) S. Tuff, T.F. Somerville, J.O. Li, T. Neal, S. De, M.J. Horsburgh, J.L. Fothergill, D. Foulkes, S. Kaye, *Prog. Retin. Eye Res.* 89 (2022) 101031.
- [8] a) P. Baranowski, B. Karolewicz, M. Gajda, J. Pluta, *Sci. World J.* 2014 (2014), 861904, 861904;  
b) K. Wang, P. Dai, N. Zhang, Y. Dong, B. Zhao, J. Wang, X. Zhang, Q. Tu, *Int. J. Biol. Macromol.* 275 (2024), 133595, 133595.
- [9] a) A.L. Onugwu, C.S. Nwagwu, O.S. Onugwu, A.C. Echezona, C.P. Agbo, S.A. Ihim, P. Emeh, P.O. Nnamani, A.A. Attama, V.V. Khutoryanskiy, *J. Contr. Release* 354 (2023) 465;  
b) C. Wang, Y. Pang, *Adv. Drug Deliv. Rev.* 194 (2023), 114721, 114721;  
c) D.R. Janagam, L. Wu, T.L. Lowe, *Adv. Drug Deliv. Rev.* 122 (2017) 31.
- [10] Z. Wang, X. Liu, Y. Duan, Y. Huang, *Biomaterials* 280 (2022) 121249.
- [11] a) Y. Wang, Y. Yang, Y. Shi, H. Song, C. Yu, *Adv. Mater.* 32 (2020) e1904106;  
b) X. Lu, X. Feng, J.R. Werber, C. Chu, I. Zucker, J.H. Kim, C.O. Osuji, M. Elimelech, *Proc. Natl. Acad. Sci. U. S. A.* 114 (2017) E9793;  
c) K.D. Patel, R.K. Singh, H.-W. Kim, *Mater. Horiz.* 6 (2019) 434;  
d) A. Serrano-Aroca, K. Takayama, A. Tunon-Molina, M. Seyran, S.S. Hassan, P. Pal Choudhury, V.N. Uversky, K. Lundstrom, P. Adadi, G. Palu, A.A.A. Aljabali, G. Chauhan, R. Kandimalla, M.M. Tambuwala, A. Lal, T.M. Abd El-Aziz, S. Sherchan, D. Barh, E.M. Redwan, N.G. Bazan, Y.K. Mishra, B.D. Uhal, A. Brufsky, *ACS Nano* 15 (2021) 8069;  
e) A. Nair, J.T. Haponiuk, S. Thomas, S. Gopi, *Biomed. Pharmacother.* 132 (2020) 110834.
- [12] a) H.S. Hsieh, R. Wu, C.T. Jafvert, *Environ. Sci. Technol.* 48 (2014) 11330;  
b) F. Vatansever, W.C. de Melo, P. Avci, D. Vecchio, M. Sadashivam, A. Gupta, R. Chandran, M. Karimi, N.A. Parizotto, R. Yin, G.P. Tegos, M.R. Hamblin, *FEMS Microbiol. Rev.* 37 (2013) 955.
- [13] a) S. Aslan, C.Z. Loebick, S. Kang, M. Elimelech, L.D. Pfefferle, P.R. Van Tassel, *Nanoscale* 2 (2010) 1789;  
b) O. Akhavan, E. Ghaderi, *ACS Nano* 4 (2010) 5731;  
c) S. Liu, L. Wei, L. Hao, N. Fang, M.W. Chang, R. Xu, Y. Yang, Y. Chen, *ACS Nano* 3 (2009) 3891;  
d) S. Kang, M. Herzberg, D.F. Rodrigues, M. Elimelech, *Langmuir* 24 (2008) 6409.
- [14] a) K.J. Lagos, D. Garcia, C.F. Cuadrado, L.M. de Souza, N.F. Mezzacappa, A.P. da Silva, N. Inada, V. Bagnato, M.P. Romero, *Wiley Interdiscip. Rev. Nanomed. Nanobiotechnol.* 15 (2023) e1887;  
b) Q. Xin, H. Shah, A. Nawaz, W. Xie, M.Z. Akram, A. Batool, L. Tian, S.U. Jan, R. Boddu, B. Guo, Q. Liu, J.R. Gong, *Adv. Mater.* 31 (2019) e1804838;  
c) F. Cui, T. Li, D. Wang, S. Yi, J. Li, X. Li, J. Hazard Mater. 431 (2022) 128597;  
d) J.H. Thurston, N.M. Hunter, K.A. Cornell, *RSC Adv.* 6 (2016) 42240.
- [15] W. Zhu, A. von dem Bussche, X. Yi, Y. Qiu, Z. Wang, P. Weston, R.H. Hurt, A. B. Kane, H. Gao, *Proc. Natl. Acad. Sci. U. S. A.* 113 (2016) 12374.
- [16] Q. Xin, Q. Liu, L. Geng, Q. Fang, J.R. Gong, *Adv. Healthcare Mater.* 6 (2017).
- [17] a) J. Chen, H. Peng, X. Wang, F. Shao, Z. Yuan, H. Han, *Nanoscale* 6 (2014) 1879;  
b) O. Akhavan, E. Ghaderi, A. Esfandiar, *J. Phys. Chem. B* 115 (2011) 6279.

- [18] a) X. Wang, Q. Shi, Z. Zha, D. Zhu, L. Zheng, L. Shi, X. Wei, L. Lian, K. Wu, L. Cheng, *Bioact. Mater.* 6 (2021) 4389;  
b) T. Pan, H. Chen, X. Gao, Z. Wu, Y. Ye, Y. Shen, *J. Hazard Mater.* 435 (2022) 128996;  
c) Y. Liu, B. Xu, M. Lu, S. Li, J. Guo, F. Chen, X. Xiong, Z. Yin, H. Liu, D. Zhou, *Bioact. Mater.* 12 (2022) 246;  
d) Z. Liu, X. Zhao, B. Yu, N. Zhao, C. Zhang, F.J. Xu, *ACS Nano* 15 (2021) 7482;  
e) S. Moayedi, W. Xia, L. Lundergan, H. Yuan, J. Xu, *Langmuir* 40 (44) (2024) 23125–23145.
- [19] a) N. Mammari, E. Lamouroux, A. Boudier, R.E. Duval, *Microorganisms* 10 (2022) 437;  
b) S. Huang, Y. Song, J.R. Zhang, X. Chen, J.J. Zhu, *Small* 19 (2023) e2207385.
- [20] a) T.Y. Ma, J. Ran, S. Dai, M. Jaroniec, S.Z. Qiao, *Angew Chem. Int. Ed. Engl.* 54 (2015) 4646;  
b) J. Park, Y. Nabae, T. Hayakawa, M.-a. Kakimoto, *ACS Catal.* 4 (2014) 3749.
- [21] a) S. Govindaraju, M. Samal, K. Yun, *Mater. Sci. Eng. C Mater. Biol. Appl.* 69 (2016) 366;  
b) H. Zhang, Q. Cheng, J.H. Lei, T. Hao, C.X. Deng, Z. Tang, S. Qu, *J. Colloid Interface Sci.* 644 (2023) 107;  
c) R. Jijie, A. Barras, J. Bouckaert, N. Dumitrescu, S. Szunerits, R. Boukherroub, *Colloids Surf. B Biointerfaces* 170 (2018) 347;  
d) Q. Wu, G. Wei, Z. Xu, J. Han, J. Xi, L. Fan, L. Gao, *ACS Appl. Mater. Interfaces* 10 (2018) 25026;  
e) H. Sun, N. Gao, K. Dong, J. Ren, X. Qu, *ACS Nano* 8 (2014) 6202.
- [22] a) X. Wang, H. Wang, J. Cheng, H. Li, X. Wu, D. Zhang, X. Shi, J. Zhang, N. Han, Y. Chen, *Chem. Eng. J.* 466 (2023);  
b) W. Dong, L. Xu, M. Chen, T. Jiang, L. Su, J. Ma, C.P. Chen, G. Zhang, *J. Mater. Chem. B* 12 (2024) 1052.
- [23] H. Miao, P. Wang, Y. Cong, W. Dong, L. Li, *Int. J. Mol. Sci.* 24 (2023) 6814.
- [24] J.F. Han, Q. Lou, Z.Z. Ding, G.S. Zheng, Q.C. Ni, R.W. Song, K.K. Liu, J.H. Zang, L. Dong, C.L. Shen, C.X. Shan, *Light Sci. Appl.* 12 (104) (2023) 104.
- [25] P. Li, F. Han, W. Cao, G. Zhang, J. Li, J. Zhou, X. Gong, G. Turnbull, W. Shu, L. Xia, B. Fang, X. Xing, B. Li, *Appl. Mater. Today* 19 (2020).
- [26] Z.M. Markovic, M.D. Budimir, M. Danko, D.D. Milivojevic, P. Kubat, D. Zmijkoski, V.B. Pavlovic, M.M. Mojsin, M.J. Stevanovic, B.M. Todorovic Markovic, *Beilstein J. Nanotechnol.* 14 (2023) 165.
- [27] a) J. Zhang, Z. Zhao, Z. Xia, L. Dai, *Nat. Nanotechnol.* 10 (2015) 444;  
b) D. Yu, E. Nagelli, F. Du, L. Dai, *J. Phys. Chem. Lett.* 1 (2010) 2165.
- [28] X. Jin, F. Gao, M. Qin, Y. Yu, Y. Zhao, T. Shao, C. Chen, W. Zhang, B. Xie, Y. Xiong, L. Yang, Y. Wu, *ACS Nano* 16 (2022) 7755.
- [29] M. Gagic, S. Kocirova, K. Smerkova, H. Michalkova, M. Setka, P. Svec, J. Pribyl, J. Masliko, R. Balkova, Z. Heger, L. Richtera, V. Adam, V. Milosavljevic, *J. Colloid Interface Sci.* 580 (2020) 30.
- [30] W. Xing, L. Ni, P. Huo, Z. Lu, X. Liu, Y. Luo, Y. Yan, *Appl. Surf. Sci.* 259 (2012) 698.
- [31] a) F. Stapleton, *Ocul. Surf.* 28 (2023) 351;  
b) M. Cabrera-Aguas, P. Khoo, S.L. Watson, *Clin. Exp. Ophthalmol.* 50 (2022) 543.
- [32] a) Y. Qian, S. Deng, Z. Cong, H. Zhang, Z. Lu, N. Shao, S.A. Bhatti, C. Zhou, J. Cheng, S.H. Gellman, R. Liu, *J. Am. Chem. Soc.* 144 (2022) 1690;  
b) Z. Pang, N. Ren, Y. Wu, J. Qi, F. Hu, Y. Guo, Y. Xie, D. Zhou, X. Jiang, *Adv. Mater.* 35 (2023) e2303562.
- [33] Z. Wu, T. Pan, D. Lin, W. Xia, J. Shan, R. Cheng, M. Yang, X. Hu, K. Nan, L. Qi, *J. Mater. Chem. B* 10 (2022) 3567.
- [34] L. Wang, Y. Wang, T. Xu, H. Liao, C. Yao, Y. Liu, Z. Li, Z. Chen, D. Pan, L. Sun, M. Wu, *Nat. Commun.* 5 (2014), 5357, 5357.
- [35] H.J. Jian, R.S. Wu, T.Y. Lin, Y.J. Li, H.J. Lin, S.G. Harroun, J.Y. Lai, C.C. Huang, *ACS Nano* 11 (2017) 6703.
- [36] a) Z.M. Markovic, M.D. Budimir Filimonovic, D.D. Milivojevic, J. Kovac, B. M. Todorovic Markovic, *J. Funct. Biomater.* 15 (2024) 73;  
b) Z.M. Markovic, D.D. Milivojevic, J. Kovac, B.M. Todorovic Markovic, *Polymers* 16 (2024) 1646.
- [37] a) S. Zhu, J. Zhang, S. Tang, C. Qiao, L. Wang, H. Wang, X. Liu, B. Li, Y. Li, W. Yu, X. Wang, H. Sun, B. Yang, *Adv. Funct. Mater.* 22 (2012) 4732;  
b) D. Qu, M. Zheng, J. Li, Z. Xie, Z. Sun, *Light Sci. Appl.* 4 (2015) e364;  
c) J. Peng, W. Gao, B.K. Gupta, Z. Liu, R. Romero-Aburto, L. Ge, L. Song, L. Alemany, X. Zhan, G. Gao, S.A. Vithayathil, B.A. Kaipparettu, A.A. Marti, T. Hayashi, J.J. Zhu, P.M. Ajayan, *Nano Lett.* 12 (2012) 844.
- [38] Q. Li, X. Shen, D. Xing, *Dyes Pigments* 208 (2023) 110784.
- [39] Z. Wu, W. Xia, L. Ou, L. Zheng, B. Hou, T. Pan, W. Sun, L.H. Koole, Y. Shao, L. Qi, *Int. J. Nanomed.* 19 (2024) 2691.
- [40] a) Y. Xu, W. Hou, K. Huang, H. Guo, Z. Wang, C. Lian, J. Zhang, D. Wu, Z. Lei, Z. Liu, L. Wang, *Adv. Sci.* 11 (2024) e2403607;  
b) L. Xie, C. Liang, Y. Wu, K. Wang, W. Hou, H. Guo, Z. Wang, Y.M. Lam, Z. Liu, L. Wang, *Small* 20 (2024) e2401253;  
c) H. Guo, Y. Lu, Z. Lei, H. Bao, M. Zhang, Z. Wang, C. Guan, B. Tang, Z. Liu, L. Wang, *Nat. Commun.* 15 (2024), 4843, 4843.
- [41] a) S. Sun, J. Chen, K. Jiang, Z. Tang, Y. Wang, Z. Li, C. Liu, A. Wu, H. Lin, *ACS Appl. Mater. Interfaces* 11 (2019) 5791;  
b) H. Zhang, H. Guo, D. Li, Y. Zhang, S. Zhang, W. Kang, C. Liu, W. Le, L. Wang, D. Li, B. Dai, *Nat. Commun.* 15 (2024), 2980, 2980.
- [42] a) B.C.M. Martindale, G.A.M. Hutton, C.A. Caputo, S. Prantl, R. Godin, J. R. Durrant, E. Reisner, *Angew Chem. Int. Ed. Engl.* 56 (2017) 6459;  
b) F. Joucken, Y. Tison, J. Lagoute, J. Dumont, D. Cabosart, B. Zheng, V. Repain, C. Chacon, Y. Girard, A.R. Botello-Méndez, S. Rousset, R. Sporken, J.-C. Charlier, L. Henrard, *Phys. Rev. B* 85 (2012).
- [43] a) D. Yan, Y. Li, J. Huo, R. Chen, L. Dai, S. Wang, *Adv. Mater.* 29 (2017) 1606459;  
b) L. Zhang, Q. Xu, J. Niu, Z. Xia, *Phys. Chem. Chem. Phys.* 17 (2015) 16733.
- [44] a) Z.M. Markovic, M. Kovacova, P. Humpolicek, M.D. Budimir, J. Vajdak, P. Kubat, M. Micusik, H. Svajdlenkova, M. Danko, Z. Capakova, M. Lehocky, B. M. Todorovic Markovic, Z. Spitalsky, *Photodiagnosis Photodyn. Ther.* 26 (2019) 342;  
b) M. Kovacova, Z.M. Markovic, P. Humpolicek, M. Micusik, H. Svajdlenkova, A. Kleinova, M. Danko, P. Kubat, J. Vajdak, Z. Capakova, M. Lehocky, L. Munster, B.M. Todorovic Markovic, Z. Spitalsky, *ACS Biomater. Sci. Eng.* 4 (2018) 3983.
- [45] a) T. Kato, Y. Yamada, Y. Nishikawa, T. Otomo, H. Sato, S. Sato, *J. Mater. Sci.* 56 (2021) 15798;  
b) K.-J. Hsu, S. Li, M. Micari, H.-Y. Chi, L.F. Villalobos, S. Huang, L. Zhong, S. Song, X. Duan, A. Züttel, K.V. Agrawal, *Nat. Energy* 9 (964) (2024) s41560-024-01556-0.
- [46] C. Hu, L. Dai, *Adv. Mater.* 31 (2019) e1804672, 1804672.
- [47] a) V.V. Panchal, C. Griffiths, H. Mosaei, B. Bilyk, J.A.F. Sutton, O.T. Carnell, D. P. Hornby, J. Green, J.K. Hobbs, W.L. Kelley, N. Zenkin, S.J. Foster, *PLoS Pathog.* 16 (2020);  
b) S. Lakhundi, K. Zhang, *Clin. Microbiol. Rev.* 31 (2018) e00020, 18.
- [48] L. Ou, X. Lv, Z. Wu, W. Xia, Y. Huang, L. Chen, W. Sun, Y. Qi, M. Yang, L. Qi, *J. Mater. Sci. Mater. Med.* 32 (2021) 20.
- [49] P.L. Zhang, L. Gopala, S.L. Zhang, G.X. Cai, C.H. Zhou, *Eur. J. Med. Chem.* 229 (2022) 114050.
- [50] Y.Y. Hu, R.R. Yadav Bheemanaboina, N. Battini, C.H. Zhou, *Mol. Pharm.* 16 (2019) 1036.
- [51] M.R. Dana, Y. Qian, P. Hamrah, *Cornea* 19 (2000) 625.
- [52] J. Lyu, M. Ge, Z. Hu, C. Guo, *Chem. Eng. J.* 389 (2020) 124456.
- [53] Y. Fang, L. Zhuo, H. Yuan, H. Zhao, L. Zhang, *Int. J. Pharm.* 639 (2023), 122945, 122945.
- [54] H. Shi, J. Zhou, Y. Wang, Y. Zhu, D. Lin, L. Lei, S. Valkal, J. Wang, X. Li, *Small* 18 (2022) e2104657, 2104657.
- [55] a) X. Du, M. Zhang, Y. Ma, X. Wang, Y. Liu, H. Huang, Z. Kang, *J. Colloid Interface Sci.* 634 (2023) 44;  
b) D.K. Ji, G. Reina, S. Guo, M. Eredia, P. Samori, C. Menard-Moyon, A. Bianco, *Nanoscale Horiz.* 5 (2020) 1240.
- [56] a) A. Aranda, L. Sequedo, L. Tolosa, G. Quintas, E. Burello, J.V. Castell, L. Gombau, *Toxicol. Vitro* 27 (2013) 954;  
b) A.R. Gliga, S. Skoglund, I.O. Wallinder, B. Fadeel, H.L. Karlsson, *Part. Fibre Toxicol.* 11 (11) (2014) 11.
- [57] a) V. Singh, A. Pal, M.P. Darokar, *Free Radic. Biol. Med.* 87 (2015) 48;  
b) J. Wang, M.F. Ansari, J.M. Lin, C.H. Zhou, Chin. J. Chem. 39 (2021) 2251.
- [58] a) B. Huang, L. Tan, X. Liu, J. Li, S. Wu, *Bioact. Mater.* 4 (2019) 17;  
b) J. Xi, G. Wei, L. An, Z. Xu, Z. Xu, L. Fan, L. Gao, *Nano Lett.* 19 (2019) 7645.
- [59] M. Varghese, M. Balachandran, *J. Environ. Chem. Eng.* 9 (2021) 106821.
- [60] a) Y. Sun, B. Xu, X. Pan, H. Wang, Q. Wu, S. Li, B. Jiang, H. Liu, *Coord. Chem. Rev.* 475 (2023) 214896;  
b) H. Ding, B. Hu, B. Zhang, H. Zhang, X. Yan, G. Nie, M. Liang, *Nano Res.* 14 (2020) 570.
- [61] a) C. Mao, Y. Xiang, X. Liu, Z. Cui, X. Yang, Z. Li, S. Zhu, Y. Zheng, K.W.K. Yeung, S. Wu, *ACS Nano* 12 (2018) 1747;  
b) J. Shan, X. Li, K. Yang, W. Xiu, Q. Wen, Y. Zhang, L. Yuwen, L. Weng, Z. Teng, L. Wang, *ACS Nano* 13 (2019) 13797.
- [62] L. Sun, Y. Zhao, H. Peng, J. Zhou, Q. Zhang, J. Yan, Y. Liu, S. Guo, X. Wu, B. Li, *J. Nanobiotechnol.* 22 (210) (2024) 210.
- [63] G. Lagana, D. Barreca, A. Calderaro, E. Bellocchio, *Curr. Med. Chem.* 26 (2019) 3242.
- [64] a) J. Prahlad, Y. Yuan, J. Lin, C.W. Chang, D. Iwata-Reuyil, Y. Liu, V. de Crecy-Lagard, M.A. Wilson, *J. Biol. Chem.* 295 (2020) 14236;  
b) G.C. Port, Z.T. Cusumano, P.R. Tumminello, M.G. Caparon, *mBio* 8 (2017) e00288, 17.
- [65] K.R. Olson, Y. Gao, *Free Radic. Biol. Med.* 135 (2019) 1.
- [66] S. Kumar, J. Saxena, V.K. Srivastava, S. Kaushik, H. Singh, K. Abo-El-Sououd, M. M. Abdel-Daim, A. Jyoti, R. Saluja, *Vaccines* 10 (2022) 1575.
- [67] R. Sun, M. Cao, J. Zhang, W. Yang, H. Wei, X. Meng, L. Yin, Y. Pu, *Int. J. Environ. Res. Publ. Health* 13 (2016) 1068.
- [68] G. Snieckute, L. Ryder, A.C. Vind, Z. Wu, F.S. Arendrup, M. Stoneley, S. Chamois, A. Martinez-Val, M. Leleu, R. Dreos, A. Russell, D.M. Gay, A.V. Genzor, B.S. Choi, A.L. Basse, F. Sass, M. Dall, L.C.M. Dollet, M. Blasius, A.E. Willis, A.H. Lund, J. Treebak, J.V. Olsen, S.S. Poulsen, M.E. Pownall, B.A.H. Jensen, C. Clemmensen, Z. Gerhart-Hines, D. Gatfield, S. Bekker-Jensen, *Science* 382 (2023) eadf3208.
- [69] L. Chen, Z. Zhang, A. Hoshino, H.D. Zheng, M. Morley, Z. Arany, J.D. Rabinowitz, *Nat. Metab.* 1 (2019) 404.
- [70] T. TeSlaa, M. Ralser, J. Fan, J.D. Rabinowitz, *Nat. Metab.* 5 (2023) 1275.